Journal of the Meteorological Society of Japan, Vol. 87A, pp. 137–151, 2009
DOI:10.2151/jmsj.87A.137

A Kalman Filter Approach to the Global Satellite Mapping of Precipitation (GSMaP) from Combined Passive Microwave and Infrared Radiometric Data

Tomoo USHIO, Kazushi SASASHIGE

Department of Electronic, Electronics and Information Engineering, Osaka University, Suita, Japan

Takuji KUBOTA

Japan Aerospace Exploration Agency/Earth Observation Research Center, Tsukuba, Japan

Shoichi SHIGE

Department of Aerospace Engineering, Osaka Prefecture University, Sakai, Japan

Ken'ichi OKAMOTO

Tottori University of Environmental Studies, Tottori, Japan

Kazumasa AONASHI

Meteorological Research Institute, Tsukuba, Japan

Toshiro INOUE

Center for Climate System Research, The University of Tokyo, Kashiwa, Japan

Nobuhiro TAKAHASHI, Toshio IGUCHI

National Institute of Information and Communications Technology, Koganei, Japan

Misako KACHI, Riko OKI

Japan Aerospace Exploration Agency/Earth Observation Research Center, Tsukuba, Japan

Takeshi MORIMOTO and Zen-Ichiro KAWASAKI

Department of Electronic, Electronics and Information Engineering, Osaka University, Suita, Japan

(Manuscript received 6 June 2008, in final form 25 November 2008)

Abstract

A system has been developed and implemented that integrates passive microwave radiometer data with infrared radiometer data in order to have high temporal (1 hour) and spatial (0.1 degree) resolution global precipitation estimates. The product (GSMaP_MVK) is produced based on a Kalman filter model that refines the precipitation rate propagated based on the atmospheric moving vector derived from two successive IR images. The proposed method was evaluated and compared with other high-resolution precipitation products and the ground-based data collected by the Automated Meteorological Data Acquisition System (AMeDAS) near Japan. It was clearly shown that the approach described in this paper performed better than without the Kalman filter, and the time series of the hourly global precipitation pattern demonstrated the potential capabilities for weather monitoring and typhoon tracking. The GSMaP_MVK product achieved a score comparable to the CMORPH and the 3B42RT products.

1. Introduction

Accurate observation of the global distribution of precipitation has long been a major scientific goal. Highly accurate time- and space-resolution estimates of precipitation on a global basis are required not only for scientific research, but also hydrologic applications, agricultural management, and weather forecasts. In spite of its importance, due to the great variability of precipitation in space and time, estimation of precipitation with sufficient accuracy and resolution on a global basis is difficult, and consequently, our knowledge of precipitation is unsatisfactory. One of the best approaches to capture global precipitation is to use data from spaceborne sensors, and we have several satellites to observe precipitation passively or actively. Among these are observations by microwave radiometers from low earth orbit satellites, which have proven to be fairly accurate.

The GPM (Global Precipitation Measurement) project is led mainly by the United States and Japan, and is now being actively promoted in Europe, France, India, and China with international cooperation. In this project, the microwave radiometers observing microwave emission from rain will be placed on many low-orbit satellites, to reduce the interval to about 3 hours in observation time for each location on the earth. However, the problem of sampling error arises if the global precipitation estimates are less than three hours. Therefore, it is necessary to utilize a gap-filling technique to generate precipitation maps with high temporal resolution, which is quite important for operational uses such as flash flood warning systems.

As is well known, mapping of global precipitation using satellite data has already been performed by numerous researchers, and an increasing number of satellite-based rainfall products, for example TMPA-RT (Huffman et al. 2007), NRLgeo (Turk and Miller 2005), PERSIANN (Sorooshian et al. 2000), CMORPH (Joyce et al. 2004), PMR (Kidd et al. 2003), and so forth, are now available in near real time over the Internet. Among them, the WCRP (World Climate Research Program) GPCP (Global Precipitation Climatology Project) has succeeded in producing precipitation estimates on a monthly 2.5-degree grid with two decades of data (1979 to present) (Adler et al. 2003), and the most recent product named TMPA (The Tropical Rainfall Measuring Mission Multisatellite Precipitation Analysis) provides 3-hour real time rainfall analysis on a 0.25-degree grid (Huffman et al. 2007). In the GPCP, the infrared radiometer, the microwave radiometer, and the data of a rain gauge on the ground are used, and the precipitation estimates are generated mainly from the visible–infrared radiometer data of the synchronous meteorological satellite based on the histogram matching for the long term with the precipitation estimates from the microwave radiometer. On the other hand, CMORPH (CPC Morphing technique) provides a global precipitation map with 30 minute 0.073 degree resolution in a different way from the GPCP. In CMORPH, two pieces of the infrared images at 30-minute time intervals are used to calculate the moving vector of the cloud, and from the moving vector image in time, the rain rates

Corresponding author: Tomoo Ushio, Department of Electronic, Electronics and Information Engineering, Osaka University, 2-1 Yamadaoka, Suita, Osaka 565-0871, Japan
E-mail: ushio@comm.eng.osaka-u.ac.jp

estimated from a microwave radiometer are propagated along with the moving vector. Thus the precipitation rates during the gap between microwave radiometer overpasses are interpolated, and decrease the sampling error. So far, the CMORPH product has showed excellent scores on a 1-day, 0.25-degree comparison in terms of correlation coefficient, RMS error, and several statistical parameters through the evaluation activities in PEHRPP (Pilot Evaluation of the High Resolution Precipitation Products).

Although the CMORPH product is one of the best products at present, there are some weaknesses. In the product, the brightness temperature determined using the infrared radiometer is used only to calculate the movement of the rainy area, and the direct transformation of the precipitation does not come from brightness temperature itself. The precipitation is estimated only from the microwave radiometers. So, when a microwave radiometer passed over a ground location again because the rain is moved without changing precipitation on the movement vector, the precision of the precipitation estimation deteriorates. In order to compensate for this, the CMORPH method introduces a backward propagation technique in time and then combines both forward and backward estimates. Thus the dynamical errors resulting from precipitation system growth and decay are reduced.

The Global Satellite Mapping of Precipitation (GSMaP) project was established by the Japan Science and Technology Agency (JST) in 2002 to produce global precipitation products with high resolution and high precision from not only microwave radiometers but also geostationary infrared radiometers. The GSMaP's goal is to develop a microwave radiometer algorithm compatible with a Precipitation Radar algorithm and eventually to produce a global precipitation map with high temporal and spatial high resolution, for instance, produced on daily basis with grid spacing of 0.25 degree of latitude by 0.25 degree of longitude, by comprehensively analyzing only satellite data. In addition, providing hourly precipitation data on a global 0.1 degree grid is added to the goals of the project, which is the subject of this paper.

When mapping global precipitation with 0.1 degree/1 hour resolution in this research, an approach similar to but different from CMORPH is taken for the mapping of precipitation. In this study, we use the moving vector derived from two successive IR images to propagate the rainy area from microwave radiometry, basically similar to CMORPH; however, we focus on the relationship between rainfall strength and IR brightness temperature T_b. In this project, the Kalman filter is applied to the rainfall rate after propagation along with the moving vector to update the rate on the IR T_b. We refer to this Kalman filter–based product as GSMaP_MVK, short for GSMaP moving vector with Kalman filter method, while the moving vector–only approach is labeled GSMaP_MV. Using this technique, a near real time system named GSMaP_MVK_RT, which simply contains only the propagation process forward in time, was developed (Noda et al. 2007). In this paper, the full system (GSMaP_MVK), which contains both the forward and backward propagation processes, is described and assessed in various time scales from other ground- and satellite-based products.

2. Data

This section describes the input data sets that are used in this study. As is stated above, the microwave radiometer (MWR) on low earth orbit (LEO) and the infrared radiometer on geostationary satellites are quite complementary with each other for monitoring the precipitation. The data used here are from the microwave radiometers in low earth orbits and the infrared radiometers in geosynchronous orbits.

The MWR sensors used in this study are SSM/I (Special Sensor Microwave/Imager), TMI (TRMM Microwave Imager), and AMSR-E (Advanced Microwave Scanning Radiometer for EOS), whose characteristics are listed in Table 1. We use the converted precipitation data from the observed brightness temperature at microwave frequencies as inputs to our system. The algorithms to retrieve the surface precipitation rate are described in Aonashi et al. (1996) and Kubota et al. (2007) for microwave radiometers. The basic idea of the Aonashi algorithm

Table 1. Characteristics of microwave radiometers used in this study.

Name	Altitude (km)	Sensor	Frequency (GHz)
TRMM	402	TMI	10, 19, 21, 37, 85
AQUA	705	AMSR-E	7, 10, 19, 24, 37, 89
DMSP-F13	803	SSM/I	19, 37, 85
DMSP-F14	803	SSM/I	19, 37, 85
DMSP-F15	803	SSM/I	19, 37, 85

is to find the optimal rain intensity that matches the brightness temperature calculated from the radiative transfer model with the observed brightness temperature at several microwave frequencies on the platform. Since we do not deal with the algorithm development of the microwave radiometer data to retrieve the surface rain rate in this paper, we do not state the algorithm techniques explicitly here.

The IR data sets used in this study are supplied from the CPC (Climate Prediction Center) of NOAA. The CPC acquires the data of the infrared radiometer from geostationary satellites (Janowiak et al. 2001) and supplies to the public the composite data sets through the Man–computer Interactive Data Access System (McIDAS; Lazzari et al. 1999). The latitude and longitude resolution of the data are 0.03635 degree (4 km at the equator). The latitude range is 60°N–60°S. The temporal resolution is about 30 minutes. In this data set, three major defects are corrected: (1) navigation error, (2) limb darkening, and (3) intersatellite calibration problems. Detailed information on these errors and associated corrections is provided by Joyce et al. (2001).

3. Methodology

The combination techniques used for producing the 0.1 degree/1 hour resolution global precipitation map in this paper are based on the morphing technique described by Joyce et al. (2004). A brief summary of the CMORPH technique is given here and then the proposed method for extending the propagation technique using a Kalman filter is described. In Fig. 1, the algorithm flow of this product (GSMaP_MVK) is shown.

3.1 Advection vector and rainfall propagation

Given two consecutive images of the IR brightness temperature with one-hour resolution at $t = 0$ and $t = 1$, the two-dimensional cross correlation coefficient can be calculated. If the image at $t = 1$ is lagged with respect to $t = 0$ image spatially in the longitudinal and latitudinal directions, the correlation is calculated for the given spatial offset. By repeating this procedure for the various offsets and searching for the horizontal offsets that yield the maximal correlation, the advection vector is determined. In this study, in order to speed up computation, the low-resolution correlation of bin-averaged images is first computed and then zoomed in recursively to obtain the optimal offsets. This stepwise procedure is significantly effective for quickly computing the shift showing the greatest correlation. In our estimation, the global advection fields in every 3.25 degree can be calculated in 5 minutes with a 3 GHz Linux computer.

Once the vector fields are obtained globally from the correlation-maximizing method described above, the rainfall area retrieved from the passive microwave

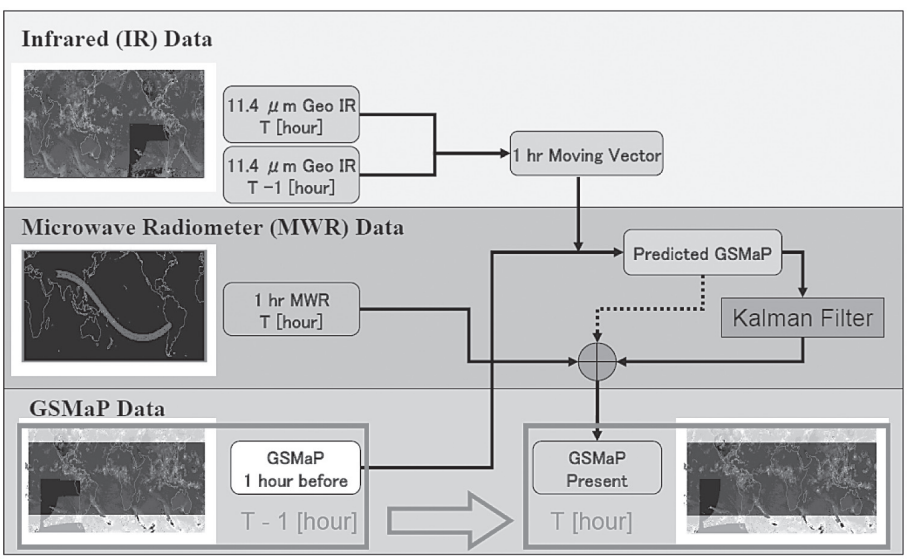

Fig. 1. Flow chart of the algorithm developed in this study.

radiometer is propagated forward in time by the advection vector derived from the IR images. In addition, the rainfall area is spatially propagated backward in time using the same advection vector used in the forward propagation. And then, the optimal estimates of rainfall rate are computed by calculating the weighted average from the forward and backward propagated rainfall rates using the inverse of temporal distance from passive microwave radiometer scan to propagation time to weight the propagated rainfall from each scan.

The spatial resolution of the GSMaP_MVK product has a minimum of 0.1 degree, while the resolution of the original IR image is 0.03635 degree at the equatorial region. This minimum bound of 0.1 degree basically comes from the resolution limit of the microwave radiometer data at high frequency, suggesting the difficulty to enhance the resolution below 10 km (at the equator).

3.2 Kalman filter

A possible main source of error with the CMORPH technique is that the advection analysis is the only process that describes the temporal variation of the precipitation system, although the weighted average called "morphing" is performed. The actual rain rate intensifies or decays during the storm life cycle, while the cloud system moves horizontally. The tracking of the cloud system can be achieved by calculating the advection vector from the consecutive IR images, but measurements that can give information on precipitation fluctuation with 1-hour resolution on a global basis are rare. Though the Geo-IR measurements are not directly related to precipitation, their information on cloud top height is available nearly all the time over the globe and is statistically correlated with surface rainfall rate with large variances. This leads us to use a Kalman filter to provide better feedback information to more accurately represent the temporal variation of precipitation system.

Let X_k be the precipitation rate at time k, which is the propagated precipitation rate forward in time. After the rain pixel is propagated along with moving vector, the predicted precipitation rate at time $k + 1$ is not necessarily the same as the actual rain rate at the time. If its uncertainty is represented as w, which is the so-called system noise, then we have

$$X_{k+1} = X_k + w. \quad (1)$$

Figure 2 shows a histogram of the uncertainty in precipitation rate after 1 hour from its propagation compared with the rain rate retrieved from the microwave radiometer. In this figure, the regional differences are ignored and all the data all over the globe are collected. Note that it is normally distributed, showing that the propagated precipitation rate can be viewed as a random variable, which enables us to take the Kalman filter approach.

At each time step, the only parameter of the

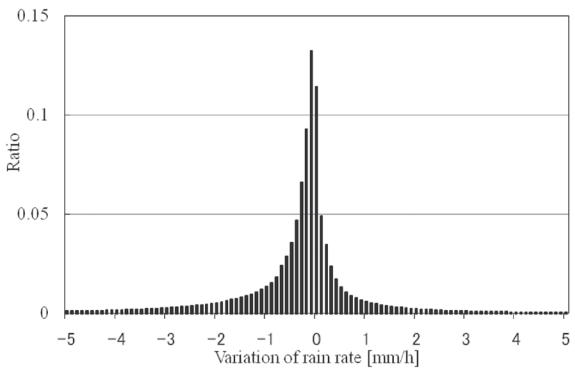

Fig. 2. Histogram of the uncertainty in precipitation rate after 1 hour from its propagation compared with the rain rate retrieved from the microwave radiometer.

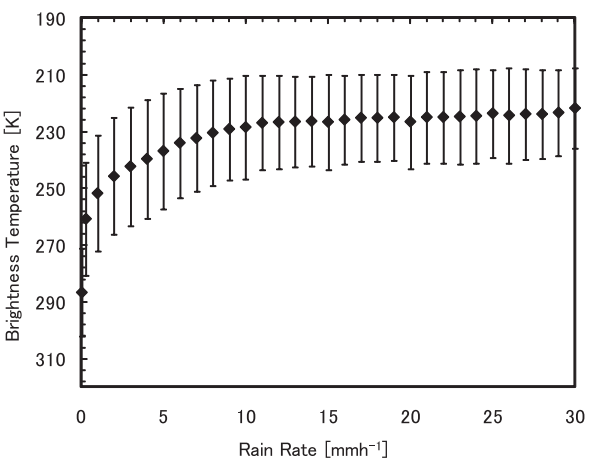

Fig. 3. Geostationary satellite IR brightness temperature (ordinate) relative to precipitation estimated from microwave radiometers (abscissa) during July 2005.

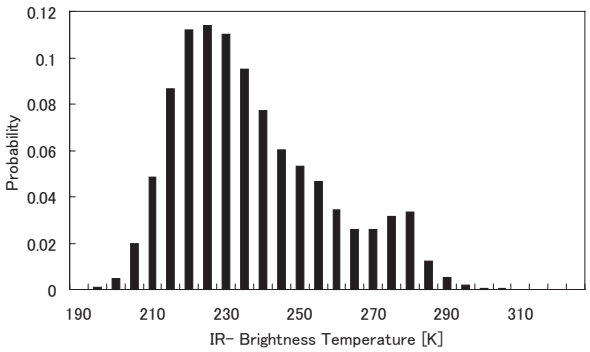

Fig. 4. Distribution of the IR brightness temperature at 3 mm h^{-1}.

measurement available to give the feedback information is the brightness temperature at the thermal-IR wavelength. In Fig. 3, the relationship between the IR brightness temperature and the precipitation rate from the microwave radiometer is shown. As seen in this figure, the brightness temperature is nonlinearly correlated with the surface precipitation rate with large variance. In Fig. 4, the histogram of the brightness temperature at the precipitation rate of 3 mm h^{-1} is shown as one example. Note that it is normally distributed. From Figs. 3 and 4, it is shown that at each time step of the propagation along with moving vector a noisy measurement of the true precipitation is made from the IR observation. Let y be the brightness temperature that is estimated from the Geo-IR measurement. Let v be the measurement error as shown in Fig. 4, which is so-called observation noise. Then we have

$$y_k = HX_k + v, \tag{2}$$

where H is a coefficient constant.

As is evident from Fig. 3, the actual relationship between IR brightness temperature (T_b) and surface precipitation rate is quite nonlinear with large

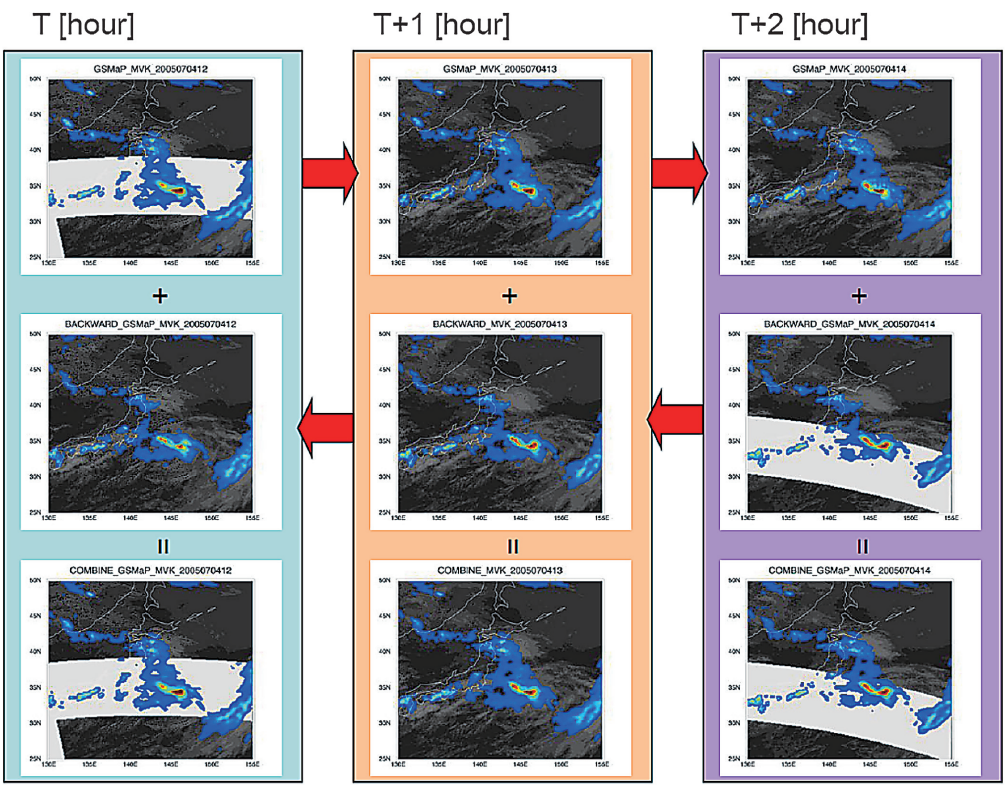

Fig. 5. Schematic illustration combining the precipitation fields forward and backward in time. The white belts denote the coverage of the microwave sensors.

variances. To apply the Kalman filter on a linear basis, the linearization approximation is needed and has been performed in every 1 mm h^{-1} at present study.

Based on equations (1) and (2), the Kalman gain is computed and then the modified precipitation rate is obtained. Here, the system under consideration is assumed to be in a steady state in order to reduce the computation cost. However, the relationships between IR T_b and the precipitation rate and between moved precipitation rate and the actual rain rate are strongly dependent on season and location. Hence, both system noise and observation noise are varying with time and location. In this study, we introduce the monthly based steady Kalman filter, which allows both the system noise and observation noise to vary from month to month. In addition, the relationship between IR T_b and precipitation rate varies from one region to the next even in the same month. In this study, to keep enough samples and to stabilize the Kalman filter, the noise tables have been created for every 10 degrees in latitude over land and ocean.

After applying the Kalman filter to the propagated rainy pixel stated above, the same propagation and Kalman filter procedure is applied to the rainy pixel backward in time as is illustrated in Fig. 5. At time t, the microwave radiometer passes over, and the rainy pixel is repeatedly propagated and the Kalman filter refines the precipitation rate as $R^f_{t,i}$ after i hours later. The revisited rainy pixel is also repeatedly propagated backward in time and the Kalman filter refines the precipitation rate as $R^f_{t,j}$, which is the estimated precipitation rate j hours before the most recent microwave radiometer overpass. In this case, the optimal estimate $\hat{R}$ is the weighted average

$$\hat{R}_t = R^f{}_{t,i}\frac{\sigma_j}{\sigma_j+\sigma_i} + R^b{}_{t,j}\frac{\sigma_i}{\sigma_j+\sigma_i}, \quad (3)$$

where sigma is the root-mean-square uncertainty in the estimates after the i or j hours from the microwave radiometer overpass.

4. Results and discussion

4.1 Example

The GSMaP_MVK has been computed for Jan. 1, 2003 to Dec. 31, 2006, and the processing still continues to obtain the long-time products. The top panel in Fig. 6 shows an example of the GSMaP_MVK product in July 15, 0 UTC 2005. Note that the global precipitation with 0.1-degree and 1-hour resolution has been produced by interpolating the rainfall rates between the microwave radiometer overpasses using the Geo-IR data sets. The global pattern of the precipitation distribution is typical for this season. While isolated scattered showers, probably from convective type rainfall, are seen in the tropics, band-type rain events appear at mid latitudes. Far south of Japan the typhoon Haitang can also be seen, which brought heavy rain recorded in the Taiwan area after a few days. The second panel in the left row in Fig. 6 shows one-day accumulation of the precipitation rate for July 3, 2005. Because the GSMaP_MVK is a relatively new technique, the 3B42 V6 (Huffman et al. 2007) is placed on the right row in Fig. 6 for a side-by-side comparison in the same scale. It is clearly shown that the both panels are basically in excellent agreement, and in the 3B42 product tiny rain pixels appear more widely scattered than in the GSMaP_MVK product. Rain events exceeding 100 mm day^{-1} are frequently seen not only in the tropics but also at the middle latitudes. Focusing on a particular event, for example, a Baiu (Japanese summer monsoon) front is seen from the Korean Peninsula to the Pacific side of the Japanese archipelago with heavy rain exceeding 100 mm day^{-1}. With this seasonal rain front, heavy rain of more than 100 mm day^{-1} is readily observed in the western part of the main island of Japan on July 3 by the Japanese Meteorological Agency and is associated with the hazardous flood that occurred there at this time. The third panels from the top in Fig. 6 show the JJA seasonal merged precipitation product in 2005 as one example. In these third panels, both products have shown good agreement, except for the ocean area near Antarctica. As is well-known, strong precipitation patterns show up on the ITCZ in the Pacific and Atlantic Oceans, with strong maxima in the eastern Pacific Ocean. Turning to the Asian Monsoon, the very heavy precipitation maximum is evident in the Bay of Bengal, with sharp contrast between ocean and land. On this sharp contrast, however, the produced product might have a tendency to underestimate the precipitation rates, particularly over land compared with the 3B42 product. In the 3B42, relatively high precipitation rates are seen over India and Bangladesh. The bottom panels in Fig. 6 display the annual precipitation map in 2005 from the GSMaP_MVK and 3B42 products. As is expected, the strong precipitation belt across the Pacific Ocean along the ITCZ is evident with peaks at the both ends

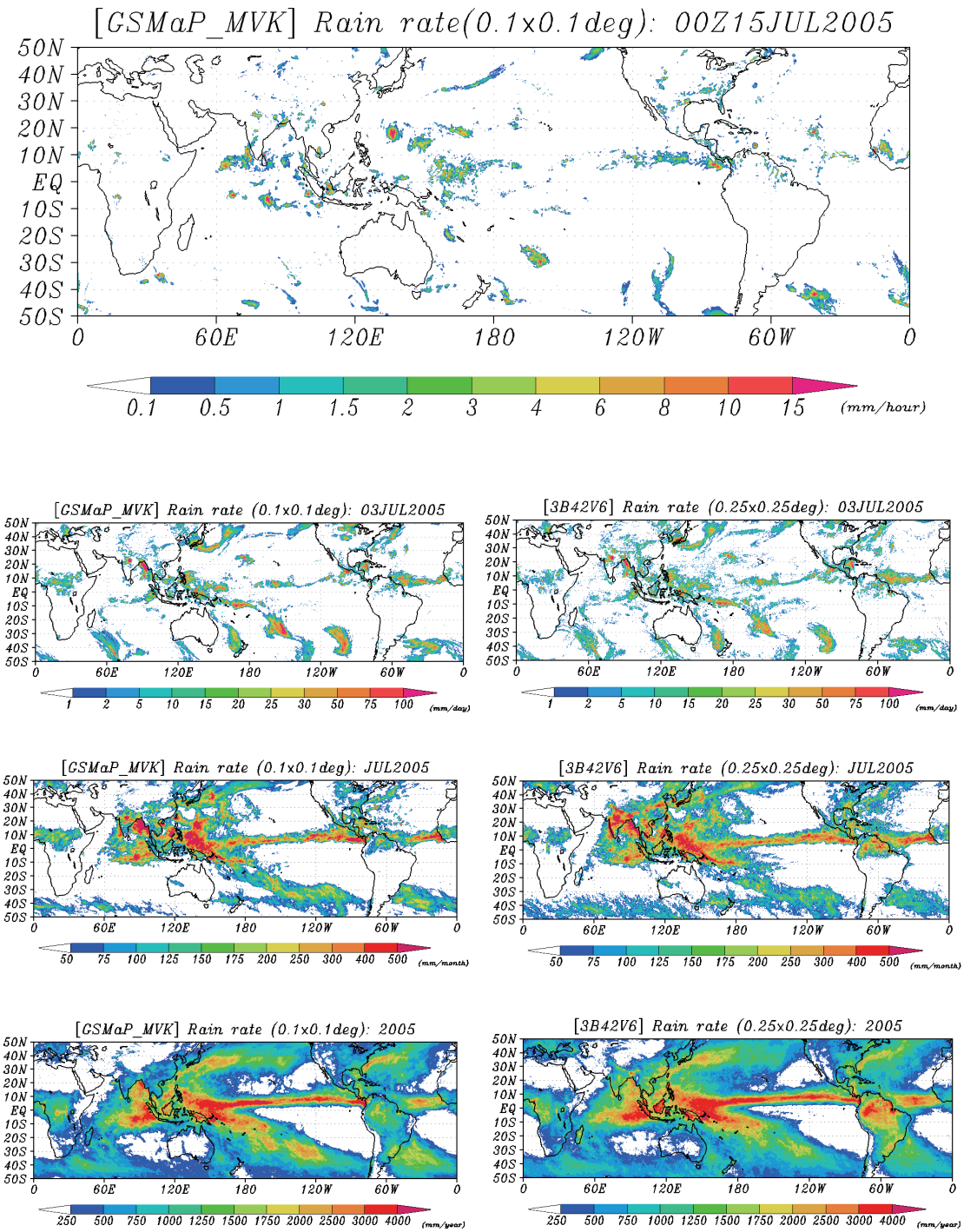

Fig. 6. Examples of the GSMaP_MVK products for various time scales. From top to the bottom, global precipitation distribution in 1 hour, daily, monthly, and annual scales are shown. Note that the area of 35–50 degrees is not covered by the TRMM/TMI, hence the number of microwave radiometer observations decreases in this region. The precipitation rate at 40–50 degrees seems to be lower in GSMaP_MVK than in the 3B42. This is partly because the algorithm of the microwave radiometer does not retrieve the rain rate if the 0 degree level is lower than 500 m.

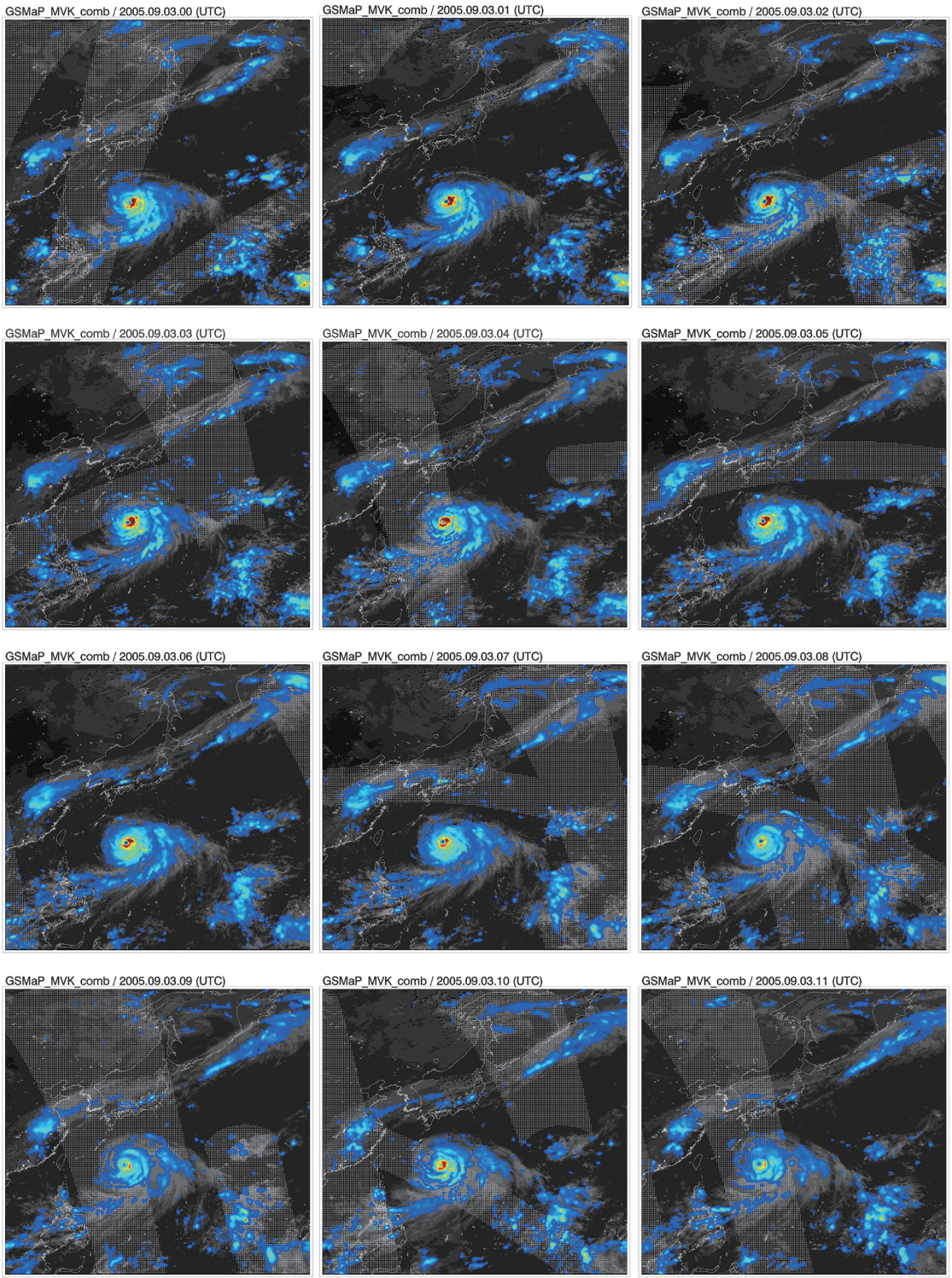

Fig. 7. Consecutive images of 12 hours with 1 hour/0.1 degree resolution from GSMaP_MVK for July 3, showing the progression of Typhoon Nabi. For each image, the color superimposed on the IR cloud image denotes the rain rate, while the grey belts denote the coverage by the various microwave sensors.

of the belt zone in both panels. In the middle latitudes, two clear storm track patterns appear near Honshu (the main island of Japan) and in the east coast of North America. All these features indicated above suggest that the final GSMaP_MVK product shows a typical precipitation pattern from sub-daily to annual scales and the developed algorithm behaves reasonably.

In order to show a particular event in finer scale, Fig. 7 shows 0.1 degree/1 hour resolution estimates of precipitation associated with the progression of Typhoon Nabi. This typhoon occurred in August 29, 2005 at the Mariana Islands, passed over Japan, and then became an extratropical cyclone in September 8, 2005 at the Kuril Islands. The twelve hours of the continuous hourly images in Fig. 7 are at the mature stage of the typhoon life cycle, and show explicitly how the pattern and amplitude of precipitation associated with the typhoon change as the typhoon propagates. The time series of the embedded precipitation distribution within the cloud pattern shows the precipitation spiraling cyclonically, and that the distribution consists of the eyewall as well as principal and secondary rainbands that occur outside the eyewall. Although the fine-scale precipitation estimates particularly with less than 1 hour resolution are quite difficult and subject to large errors on a global basis, the overall pattern of the typhoon looks typical showing that the produced product can be useful for typhoon tracking and monitoring. It is quite interesting to investigate how the eyewall and the rainbands propagate and develop in a fine time scale, which will be a theme of a future paper.

4.2 Assessment and validation

An initial validation was carried out using microwave radiometer data for the period of July 2005. In the proposed approach, precipitation estimates from microwave radiometers are propagated by moving vectors derived from Geo-IR data, and the Kalman filter modification is applied to the propagated rain rate. This procedure is repeated forward in time until the next microwave radiometer overpasses. When the next microwave radiometer arrives, the propagated rain pixels are overwritten by precipitation estimates from an updated microwave scan. At the time of this overwrite, there are two simultaneous estimation of precipitation: one is from the Kalman filter output and another is from the newest passive microwave radiometer. Since we have precipitation estimates with and without Kalman filter (i.e., moving vector only), we can quantitatively estimate the error of the proposed method compared with the moving vector only approach if the precipitation estimates from the updated microwave scans are regarded as truth. An advantage of this assessment is that a more general evaluation is possible than that of the ground-based radar data because the validation area is not restricted in any particular area or time like ground-based rain gauges or radars.

Figure 8 shows the correlation of GSMaP_MV and GSMaP_MVK precipitation estimates using only the forward process with microwave radiometer estimation over one month (July 2005) as a function of time from the past microwave overpass in the tropics (0–10°N) and the extratropics (20–30°N) over land and ocean. It is shown how the correlation coefficient behaves as a function of time after the past microwave overpass. When the Kalman filter is applied to the propagated rain pixels, a difference between with and without Kalman filter is not seen in one or two hours after the last microwave overpasses. However, in several hours later, the proposed Kalman filter method tends to make a difference. For example, at four hours later, the correlation coefficient at this time over ocean in tropics shows about 0.35 for GSMaP_MVK, while the GSMaP_MV shows 0.23. This difference tends to be larger as the time passes, demonstrating the beneficial effect of the proposed Kalman filter approach compared with the moving vector only approach. This trend is common in all cases in Fig. 8. Concerning at the latitude and land/ocean dependence, the correlations over ocean are better than over land, probably due to the microwave radiometer algorithm performance. It seems that the extratropical case over ocean behaves better than the tropics case over ocean. However, overall, the tropical and extratropical difference is not so large. In the horizontal axis of this figure, 6 hours from the last microwave overpass is chosen as the maximum value, because the five microwave radiometers (TMI, AMSR-E, and SSM/Is) can cover about 88% of the whole earth in a 6-hour interval, while 25% is covered in 1-hour intervals. If we process the data before the TRMM launching, the available microwave sensors are SSM/Is only and the really observable area at a certain time interval decreases by least several tens of percent, with the result that the effective time of the Kalman filter approach will increase.

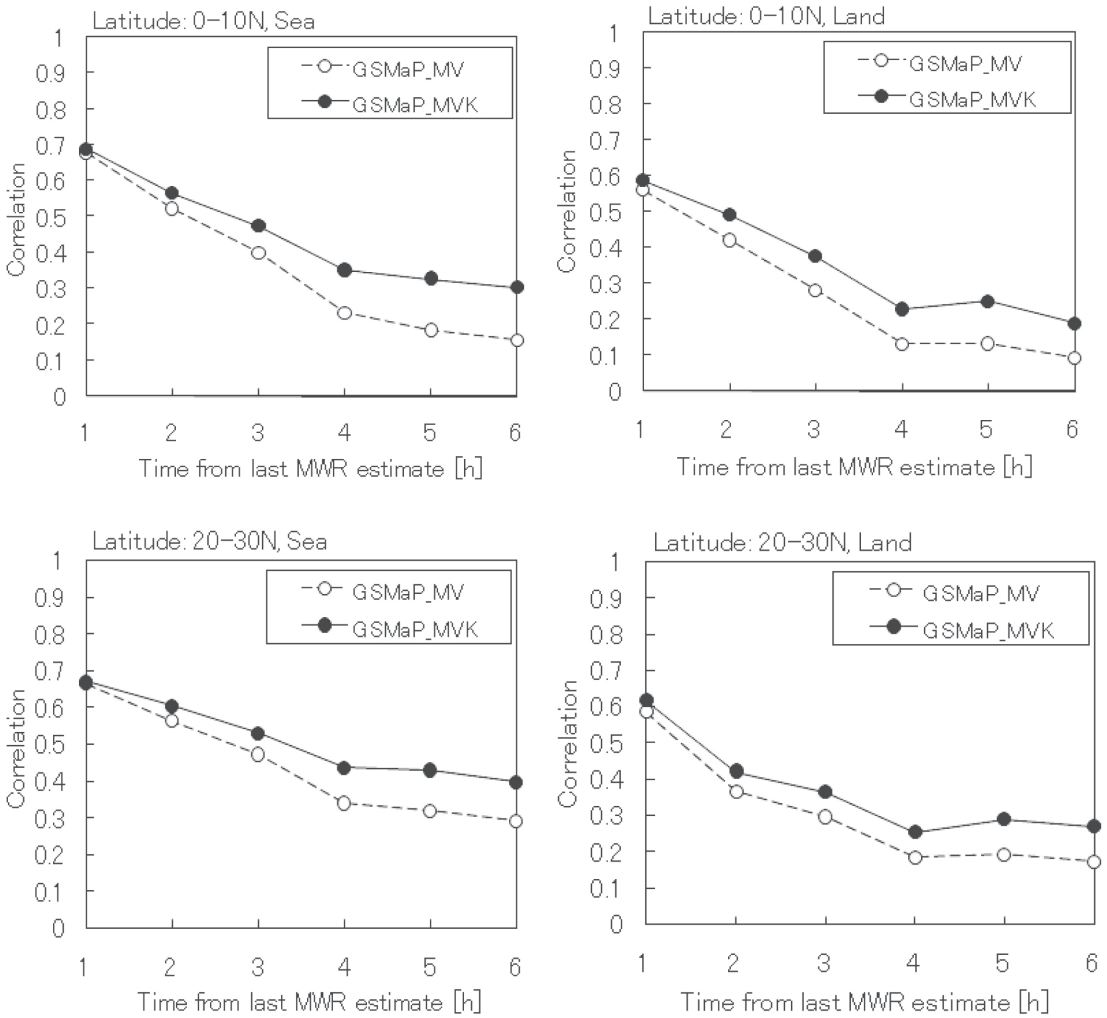

Fig. 8. Correlation coefficient between GSMaP and precipitation estimated from microwave radiometers for the period of July 2005 in the tropics and the extra-tropics over land and ocean. Solid line denotes the Kalman filter method, while the dotted line denotes the moving vector only method.

The validation results so far have been for the assessment of the proposed technique. The actual GSMaP_MVK final product, which has one hour/0.1 degree resolution, is composed of many precipitation estimates not only from the microwave radiometer but also from the Kalman filter modification at various hours after the last microwave radiometer overpasses. A comparison of the near real time prodproductuct (GSMaP_MVK_RT) with RADAR-AMeDAS has been done in Noda et al. (2007). Taking the discussion one step further in this paper, the GSMaP_MVK product, which includes both forward and backward process in time, is validated and assessed in several temporal and spatial scales. First, the GSMaP_MVK product is evaluated on an hourly scale using the RADAR-AMeDAS data sets on a 0.1 degree/1 hour basis. Second, the daily scale evaluation is carried out as a part of the IPWG (International Precipitation Working Group) activities (Ebert et al. 2006). Finally, monthly scale cross comparison with the GPCP is stated on a global basis.

Figure 9 shows a typical result consisting of a time series of the 0.1 degree/1 hour resolution precipitation estimates for 12 hours in July 25 2005 as well as the RADAR-AMeDAS composites and IR brightness

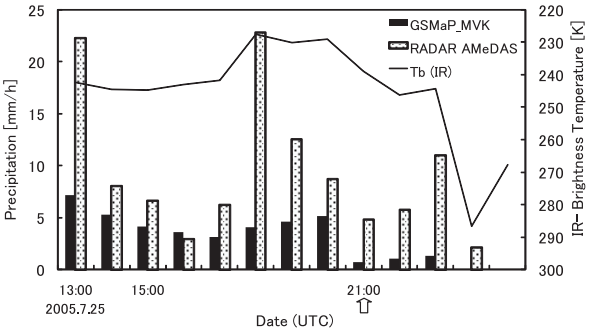

Fig. 9. Time series of the 1 hour precipitation from the RADAR-AMeDAS (dotted bars) and GSMaP_MVK (black bars) together with the IR brightness temperature (solid line) at the pixel at 35°N, 124°E. The microwave estimates are at 21:00 and 0:00. The arrow at 21:00 indicates the time of the microwave radiometer overpass.

temperature in a moving coordinate with the atmospheric motion vector. In general, it is shown that the GSMaP_MVK can correctly catch the rainfall occurrences and adjust the rainfall rates in reference to the IR brightness temperature. However, the GSMaP_MVK product has the tendency to underestimate the precipitation intensity, particularly for strong rainfall rates more than 10 mm h^{-1}. This is probably because this sudden increase in rain rate did not reflect the IR brightness temperature in this time scale.

The scattergram between the RADAR-AMeDAS and GSMaP_MVK for July 2005 in logarithmic scale is shown in Fig. 10. In this figure, the unit is 10log(rain rate in mm h^{-1}) [dBR]. The left panel is with the original 1 hour/0.1 degree resolution and the right panel is with averaged 3 hour/0.25 degree resolution. These panels show that the finer scale estimates show significant scatter, and it is anticipated that the 1 hour/0.1 degree plots show more uncertainties than the 3 hour/0.25 degree plots. In left panel, the high-density region spreading through the vertical axis from –4 dBR in abscissa axis comes from the discrete observation of the RADAR-AMeDAS. The dotted line is the one-to-one line in both panels. The correlation coefficients are 0.44 and 0.65 for the 1 hour/0.1 degree and 3 hour/0.25 degree resolution, respectively, and the monthly mean precipitation rate is 0.17 mm h^{-1} for the GSMaP_MVK and 0.23 mm h^{-1} for the RADAR-AMeDAS, suggesting that the GSMaP_MVK estimates matches well to the RADAR-AMeDAS estimates and tends to underestimate large precipitation values. At the moment, this will be partly because the current algorithm of the microwave radiometer does not

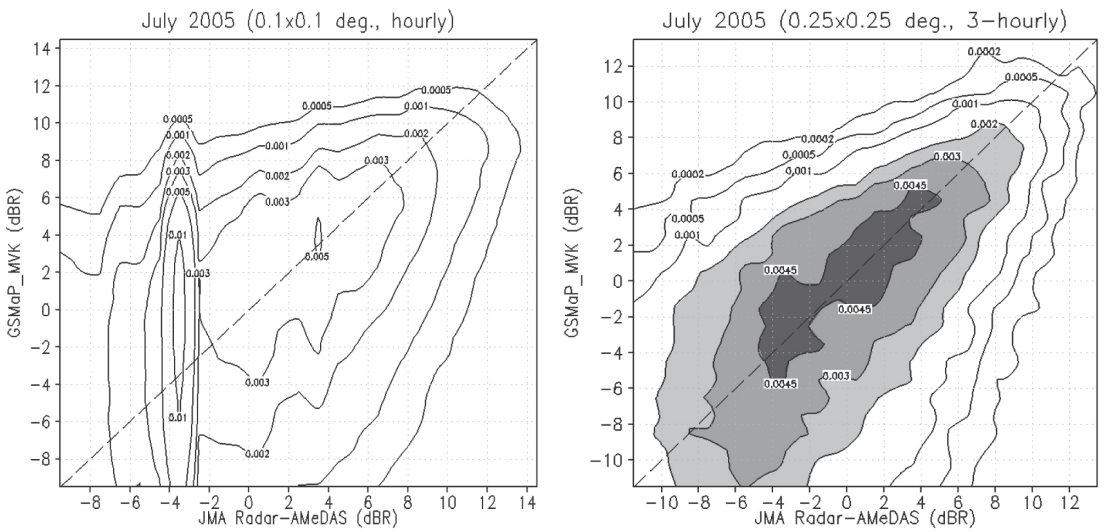

Fig. 10. Scatter plots comparing the hourly precipitation estimates from GSMaP_MVK with RADAR-AMeDAS with 1 hour/0.1 degree (left panel) and 3 hour/0.25 degree (right panel) resolution.

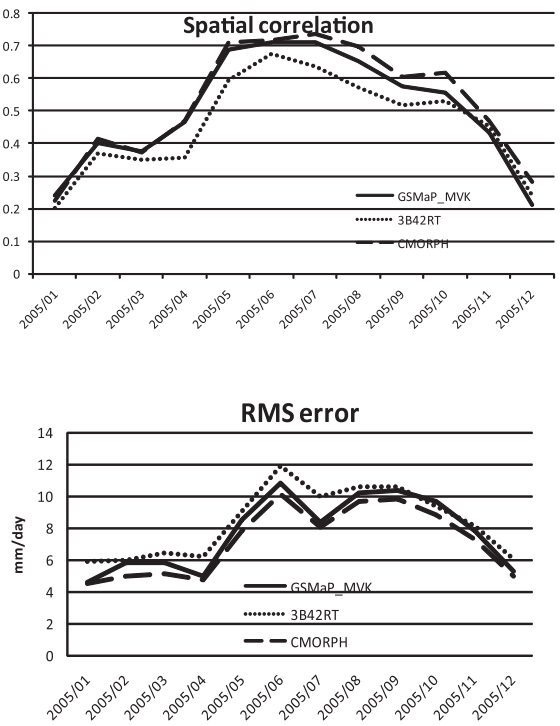

Fig. 11. Time series of correlation coefficient between the GSMaP_MVK, CMORPH, 3B42RT, and RADAR-AMeDAS data during 2005.

include the topographical effect and the current IR observation cannot be made with resolution of less than one hour.

To validate the daily rainfall estimates, the IPWG/PEHRPP validation data (Ebert et al. 2007) were

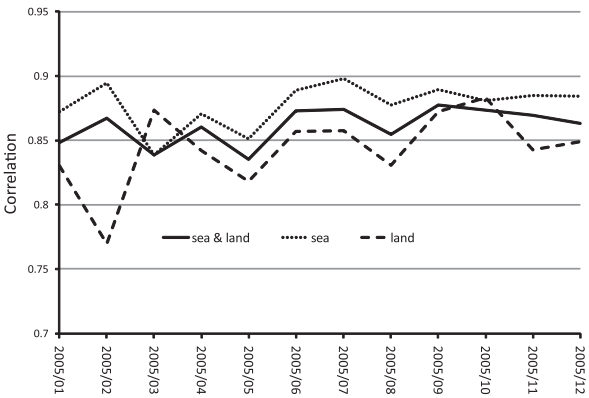

Fig. 12. Time series of the monthly correlation between the GPCP and GSMaP_MVK over land and ocean.

used in this study. The validation sites list the several statistical values; by picking up these values a time series evaluation of the GSMaP_MVK product and some other products on a daily basis is possible. Thus Fig. 11 shows a time series of monthly averaged daily correlation coefficients and RMSEs for the GSMaP_MVK, 3B42RT, and CMORPH products over Japan in 2005. On the whole, better correlation is obtained during the summer than the winter in every product listed here. In July the correlation coefficient shows nearly 0.7, while in January the correlation coefficient drops only about 0.2. Probably this is partly because of the difficulty of the snow/rain retrieval in passive microwave radiometer algorithms. Generally, the GSMaP and CMORPH products show better scores

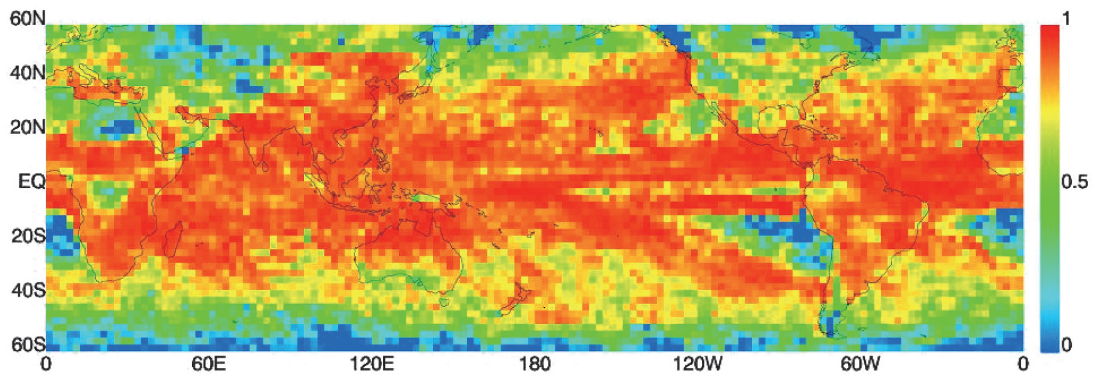

Fig. 13. A map of correlation of GSMaP_MVK against GPCP at each grid point for the period 2003–2006.

in terms of correlation and RMSE than the 3B42RT, indicating that the IR moving vector approach is basically superior to the method that converts the IR brightness temperature to precipitation rates. The CMORPH and GSMaP products have quite similar correlation overall, and it appears that the CMORPH shows a slightly better score than the GSMaP_MVK in spite of the Kalman filter. Probably it is because the CMORPH uses the NOAA/AMSU microwave sounder data in addition to the microwave radiometer data, while the GSMaP_MVK uses only the microwave radiometer data. On the detailed analysis with this daily resolution, Kubota et al. (this issue) provides a comprehensive review.

It is usually difficult to validate the high-resolution product on a global basis, because the high-resolution ground gauge network is not necessarily available all over the world. In order to assess the GSMaP_MVK product on a global basis, the cross comparison has been done using the GPCP product, which is well validated and calibrated from GPCC data sets. In Fig. 12, correlation validation of monthly 1 degree GSMaP_MVK against GPCP analyses is presented for Jan.–Dec. 2005. Generally the GSMaP_MVK over ocean performs better than over land for the entire period, probably because the algorithm of the microwave radiometers shows a better performance over ocean than over land (Kubota et al. 2007). The total correlation including ocean and land is better than 0.85 through the year, suggesting that the GSMaP_MVK can be used for climatological studies. In this comparison, the seasonal variation in terms of correlation is not clear. In order to see where around the globe the GSMaP_MVK data sets agree or disagree, a map of correlation of GSMaP_MVK against GPCP is shown in Fig. 13. Correlation calculations are performed for the time series of the 48 months precipitation at each grid point for the period of 2003 to 2006. Note that the higher correlation appears mainly on the middle to lower altitude while the correlation drops near the polar region.

5. Summary and conclusions

An algorithm has been developed to map global precipitation distribution with 0.1 degree/1 hour resolution by integrating the data from the LEO microwave radiometers and the GEO infrared radiometers. The algorithm (GSMaP_MVK) uses the Kalman filter to update the precipitation rate after propagating the rain pixels along with the atmospheric motion vector derived from the successive IR images. The distribution and amplitude of the global precipitation pattern is generally consistent with the early studies. The proposed approach showed a better score than the technique without the Kalman filter. The correlation coefficient was 0.1 better than without the Kalman filter about 4 hours after the last microwave overpasses, and the RMS error was improved about 0.1 mm h^{-1} with the Kalman filter technique. The IPWG daily comparisons with the radar rain gauge network in Japan showed one of the highest scores among the typical global precipitation products.

One of the disadvantages of this product is the difficulty of describing the initiation of precipitation between the microwave radiometer overpasses. The current algorithm propagates and applies the Kalman filter only for the rainy pixels identified by the microwave radiometer algorithm. Because of this, the rainy area appears in the product only after the microwave radiometer overpasses and observes the area. This may be resolved by considering the dual channel observation (Inoue 1987) or WV channel (Ohsawa et al. 2001); that is for future work.

Apparently, more work is needed to explicitly evaluate the quality of the data products in several time and spatial scales using the different data sources, and to improve the quality of the algorithm. Since the precipitation rate produced by the proposed method strongly depends on the precipitation estimates retrieved from the microwave radiometer data, careful analysis is needed to evaluate the sources of the errors.

Acknowledgment

This work is conducted as a part of the Global Satellite Mapping of Precipitation (GSMaP) project supported by the Core Research for Evolutional Science and Technology (CREST) program of Japan Science and Technology (JST), and TRMM/RA from JAXA.

References

Adler, R. F., G. J. Huffman, A. Chang, R. Ferraro, P. P. Xie, J. Janowiak, B. Rudolf, U. Schneider, S. Curtis, D. Bolvin, A. Gruber, J. Susskind, P. Arkin, and E. Nelkin, 2003: The version-2 Global Precipitation Climatology Project (GPCP) monthly precipitation analysis (1979–present). *J. Hydrometeor.*, **4**, 1147–1167.

Aonashi, K., A. Shibata, and G. Liu, 1996: An over-

ocean precipitation retrieval using SSM/I multichannel brightness temperature. *J. Meteor. Soc. Japan,* **74**, 617–637.

Ebert, E., J. Janoviak, and C. Kidd, 2007: Comparison of near-real-time precipitation estimates from satellite observations and numerical models. *Bull. Amer. Meteor. Soc*., **88**, 47–64.

Huffman, G., R. F. Adler, D. T. Bolvin, G. Gu, E. J. Nelkin, K. P. Bowman, Y. Hong, E. F. Stocker, and D. B. Wolff, 2007: The TRMM Multisatellite Precipitation Analysis (TMPA): Quasiglobal, muultiyear, combined-sensor precipitation estimates at fine scales. *J. Hydrometeor.*, **8**, 38–55.

Inoue, T., 1987: A cloud type classification with NOAA 7 Split-Window measurements. *J. Geophys. Res*., **92**, 3991–4000.

Janowiak, J., R. J. Joyce, and Y. Yahosh, 2001: A real-time global half-hourly pixel-resolution IR dataset and its applications. *Bull. Amer. Meteor. Soc*., **82**, 205–217.

Joyce, R., J. E. Janowiak, and G. J. Huffman, 2001: Latitudinally and seasonally dependent zenith-angle corrections for geostationary satellite IR brightness temperatures. *J. Appl. Meteor*., **40**, 689–703.

Joyce, R., J. E. Janowiak, P. A. Arkin, and P. Xie, 2004: CMORPH: A method that produces global precipitation estimates from passive microwave and infrared data at high spatial and temporal resolution. *J. Hydrometeor*., **5**, 487–503.

Kidd, C., D. Knoveton, M. Todd, and T. Bellerby, 2003: Satellite rainfall estimation using combined passive microwave and infrared algorithm. *J. Hydrometeor*., **4**, 1088–1104.

Kubota, T., S. Shige, H. Hashizume, K. Aonashi, N. Takahashi, S. Seto, M. Hirose, Y. Takayabu, K. Nakagawa, K. Iwanami, T. Ushio, M. Kachi, and K. Okamoto, 2007: Global precipitation map using satellite-borne microwave radiometers by the GSMaP project: Production and validation. *IEEE Trans. Geosci. Remote Sens*., **45**, 2259–2275.

Kubota, T., T. Ushio, S. Shige, S. Kida, M. Kachi, and K. Okamoto, 2009: Verification of high-resolution satellite-based rainfall estimates around Japan using a gauge-calibrated ground-radar dataset, *J. Meteor. Soc. Japan*, **87A**, 203–222.

Lazzara, M. A., J. M. Benson, R. J. Fox, D. J. Laitsch, J. P. Rueden, D. A. Santek, D. M. Wade, T. M. Whittaker, and J. T. Young, 1999: The man computer interactive data access system: 25 Years of interactive processing. *Bull. Amer. Meteor. Soc*., **80**, 271–284.

Noda, S., K. Sasashige, D. Katagami, T. Ushio, T. Kubota, K. Okamoto, Y. Iida, S. Kida, S. Shige, S. Shimomura, K. Aonashi, T. Inoue, T. Morimoto, and Z.-I. Kawasaki, 2007: Mapping global precipitation with satellite borne microwave radiometer and infrared radiometer using Kalman filter. *J. Remote Sens. Soc. Japan*, **27**, 474–482, (in Japanese).

Ohsawa, T., H. Ueda, T. Hayashi, A. Watanabe, and J. Matsumoto, 2001: Diurnal variation of convective activity and rainfall in tropical Asia, *J. Meteor. Soc. Japan*, **79**, 333–352.

Sorooshian, S., K. Hsu, G. Gao, H. Gupta, B. Imama, and D. Braitwaite, 2000: Evaluation of PERSIANN system satellite-based estimates of tropical rainfall. *Bull. Amer. Meteor. Soc*., **81**, 2035–2046.

Turk, J., and S. Miller, 2005: Toward improving estimates of remotely sensed precipitation with MODIS/AMSR-E blended data techniques. *IEEE Trans. Geosci. Remote Sens*., **43**, 1059–1069.